Stability Analysis of AC–DC Full-Bridge Converters With Reduced DC-Link Capacitance

Rafael Z. Scapini, *Student Member, IEEE*, Lucas V. Bellinaso, *Student Member, IEEE*, and Leandro Michels, *Member, IEEE*

***Abstract*—Voltage ripple in single-phase ac–dc converters is usually disregarded to design the dc-link voltage control system, since large dc-link electrolytic capacitors are typically employed. However, replacement of electrolytic capacitors by film capacitors has been widely considered for increasing reliability. Consequently, due to cost constraints, such replacement usually employ low capacitance and may be combined with fast dc-bus voltage controllers. This paper shows that the conventional linear time-invariant (LTI) model may not represent the real converter behavior for reduced capacitance and/or faster controllers, leading to poor system performance or even instability. In this way, for any of these cases, the linear time-periodic (LTP) model is highly encouraged for stability and transient analysis as a tool for the controller design. Experimental results confirm that stability margins are precisely obtained from the LTP model but may not from the LTI model. Finally, this paper also compares both LTI and LTP models while considering the control gain and the dc-bus capacitance size. It is graphically revealed that the phase margin of the LTI model diverges from the LTP model for low dc-bus capacitances and high control gains.**

***Index Terms*—AC–DC power conversion, dc voltage control, generalized Nyquist stability, harmonic theory, linear time-periodic (LTP) models, power conversion harmonics.**

I. Introduction

POWER factor correction (PFC) ac/dc converters have been widely used in most of the electronic devices. International harmonic regulations have widespread use ranging from low-power electronic ballast to high-power drivers [1]. Most of these converters have been used in low-cost single-phase applications, where price constraints are a highly relevant issue.

Single-phase ac/dc converters have pulsating input energy conversion, which produces some low-order noncharacteristic harmonics in the dc link. In order to obtain a regulated output voltage, these converters normally include bulky electrolytic dc-link capacitors to filter out low-frequency voltage ripple [1], [2].

In recent years, one important trend in the design of ac/dc converters has been to increase their lifetime. Since electrolytic capacitors reduce the system reliability because of the short lifetime [3], [4], their replacement by long-lifetime film capacitors has been considered in many cases [5], [6]. However, as film capacitors have lower power density and higher cost, many designs have been done with small dc-link capacitance.

PFC ac/dc converters with a small dc-link capacitance have low stored energy in the dc link. In these cases, fast dynamic response dc-link voltage control must be used in order to avoid a significant dc-link voltage fluctuation due to abrupt load changes [1], [5]. Several design techniques have been presented to improve the dc-link voltage dynamic response of single-phase PFC converters without compromising on the input power factor (PF) [7]–[12]. However, the combination of fast dynamic response ac/dc dc-link voltage control with a small dc-link capacitance may lead to poor system performance and instability. This occurs due to interactions of dc-link low-frequency voltage ripple with the feedback control loop.

Conventional linear time-invariant (LTI) dc-link voltage models of PFC converters do not describe the pulsating input power processing. Since these models approximate the converter's dynamic by a dc–dc power conversion, they are only suitable when the converter has bulky dc-link capacitance or low control bandwidth [13], [14]. The input–output frequency conversion that occurs in PFC converters is suitably described by the modulation theory. Linear time-periodic (LTP) models are suitable to describe such dynamic systems, since they model the frequency modulations and are suitable to analyze the spectral interactions due to the feedback [14]. LTP representation has been used to analyze the stability of this type of power converters, such as dc–dc boost converters [15], diode rectifiers [16], buck–boost converters [17], three-phase thyristor-controlled reactors [18], unbalanced three-phase voltage-source converters [19], and wind turbines [20], among others.

Analogous to Laplace transfer functions (TF), the LTP systems can be represented in the frequency domain by harmonic transfer functions (HTF). The HTF modeling methodology is based on the linear independence of the exponential terms of the model, well known under exponentially modulated signal theory [21]–[26]. HTF models can be used to design the controller as well as to analyze the stability using the generalized Nyquist criterion [27]–[30].

Manuscript received June 13, 2016; revised December 5, 2016; accepted February 10, 2017. Date of publication February 23, 2017; date of current version October 6, 2017. This work was supported by the Conselho Nacional de Desenvolvimento Científico e Tecnológico (CNPq), by the Coordenação de Aperfeiçoamento de Pessoal de Nível Superior (CAPES), and by the Centrais Hidrelétricas de Carazinho (Eletrocar). The work of L. Michels was supported by a research grant of CNPq, Brasil (308812/2015-8). Recommended for publication by Associate Editor L. Huber.

R. Z. Scapini is with the Federal Institute of Rio Grande do Sul, Ibirubá 98200-000, Brazil, and also with the Federal University of Santa Maria, Santa Maria 97105-900, Brazil. (e-mail: scapinirz@gmail.com).

L. V. Bellinaso and L. Michels are with the Power Electronics and Control Research Group, Federal University of Santa Maria, Santa Maria 97105-900, Brazil (e-amil: lucas@gepoc.ufsm.br; michels@gepoc.ufsm.br).

Color versions of one or more of the figures in this paper are available online at http://ieeexplore.ieee.org.

Digital Object Identifier 10.1109/TPEL.2017.2672982

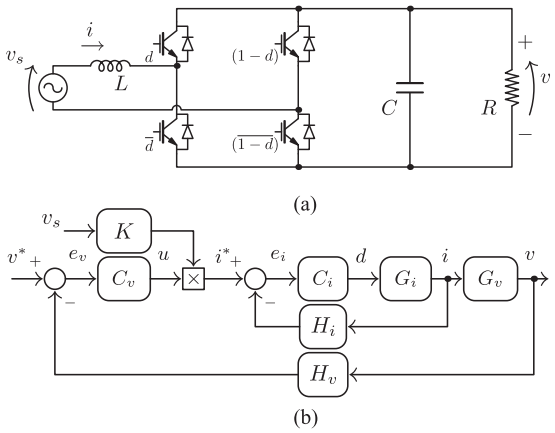

Fig. 1. AC–DC full-bridge rectifier. (a) Electrical power circuit. (b) Closed-loop control block diagram.

In contrast to the Floquet analysis, that only results in a yes or no answer to the question of stability, this paper prefers using the Wereley methodology that is based on the open-loop HTF, since it may be used as a compensator synthesis tool. In this way, the closed-loop stability margins can be addressed from its open-loop analysis.

This paper proposes to investigate the stability of an ac–dc full-bridge converter with PFC with reduced dc-link capacitance considering both conventional LTI and LTP approaches. Complete LTI and LTP models are presented in the frequency domain, and the stability is analyzed considering both approaches. Also, a design example is presented of an ac–dc full-bridge converter with reduced dc-link capacitance and high-frequency outer voltage loop bandwidth. Experimental validation demonstrates that the LTP approach accurately models the converter stability. Finally, the impact of the dc-link capacitance on the system stability is analyzed, where it is demonstrated that LTI models may no longer be valid when using a reduced dc-bus capacitance or a dc-bus voltage control with high-frequency bandwidth.

II. Problem Description and Modeling

Consider the single-phase ac–dc full-bridge converter with PFC shown in Fig. 1(a). The converter has four switches, where the input inductor L reduces input current ripple and the output capacitor C reduces dc-link voltage 100/120-Hz ripple. A sinusoidal pulse width modulation technique is used to obtain the switch signals by modulating the duty cycle d. The output is connected to a resistive load R, while the single-phase grid v_s is considered a low-impedance sinusoidal source.

A conventional PFC control structure of an ac–dc full-bridge converter is shown in Fig. 1(b). This control scheme is based on two control layers: an inner current loop to ensure a sinusoidal input current waveform, and an outer voltage loop for dc-link voltage regulation. The outer loop compensator C_v regulates the average dc voltage v by calculating the magnitude of current reference u. PFC is achieved from voltage v_s by

$$i^*(t) = Kv_s(t)u(t) \tag{1}$$

where i^* is the current reference and has the same shape of v_s.

Additionally, the duty cycle d is the control action of the inner loop compensator C_i to make the current i track its reference i^*. The blocks G_i and G_v denote the current i and voltage v plants, respectively. The sensor gains H_i and H_v are also illustrated for current and voltage measures, respectively.

Disregarding the modulation frequency f_s and their harmonic components, the model for the full-bridge is obtained for averaged values in the switching period T_s. In this way, all measured values are written in terms of the averaged input voltage, defined as

$$v_s(t) = \frac{1}{T_s}\int_t^{t+T_s} v_{\text{in}}(\tau)\, d\tau \tag{2}$$

where $v_{\text{in}} = V_{\text{RMS}}\sqrt{2}\cos(\omega_1 t)$ is the instantaneous sinusoidal input voltage.

Then, since the control action d is defined in the interval [0, 1], the nonlinear model state equation takes a well-known form [31]–[33]

$$\begin{bmatrix}\dot{i}(t)\\ \dot{v}(t)\end{bmatrix} = \begin{bmatrix}0 & \dfrac{1-2d(t)}{L}\\ \dfrac{2d(t)-1}{C} & \dfrac{-1}{RC}\end{bmatrix}\begin{bmatrix}i(t)\\ v(t)\end{bmatrix} + \begin{bmatrix}\dfrac{1}{L}\\ 0\end{bmatrix} v_s(t). \tag{3}$$

A. Open-Loop LTP Small-Signal Model

One may observe in the control structure of Fig. 1(b) that the current reference i^* is a time-periodic function, and then, its behavior should be included in the LTP model. This implies that the inner current loop should also be included in the open-loop small-signal model. Thus, the presented LTP model describes the perturbation behavior from u to v.

The current control is an LTI state-space equation that defines the duty cycle d based on the current error e_i given by

$$\dot{x_i}(t) = A_i x_i(t) + B_i e_i(t) \tag{4}$$

$$d(t) = C_i x_i(t) + D_i e_i(t) \tag{5}$$

where the current error $e_i(t) = Kv_s(t)u(t) - H_i i(t)$ is determined by the control scheme.

The full-bridge complete model from u to v is, then, determined by substituting the output current control function (5) into (3), and the current control states x_i of (4) are included in the nonlinear full-bridge model in (3). Then, we obtain

$$\begin{aligned}
\dot{x_i}(t) &= A_i x_i(t) - B_i H_i i(t) + B_i K v_s(t) u(t)\\
\dot{i}(t) &= \frac{1}{L}v(t) - \frac{2C_i}{L}x_i(t)v(t) + \frac{2D_i H_i}{L}i(t)v(t) +\\
&\quad - \frac{2D_i K}{L}v_s(t)v(t)u(t) + \frac{1}{L}v_s(t)\\
\dot{v}(t) &= -\frac{1}{RC}v(t) + \frac{2C_i}{C}x_i(t)i(t) - \frac{2D_i H_i}{C}i^2(t) +\\
&\quad - \frac{1}{C}i(t) + \frac{2D_i K}{C}v_s(t)i(t)u(t).
\end{aligned} \tag{6}$$

The linear-time version of (6) is determined by applying a perturbation signal around the nominal value for each variable. The biggest difference between LTI and LTP methodologies is that LTP has time-varying nominal values, typically sinusoidal. In this way, the current control states $x_i(t) = X_i(t) + \tilde{x_i}(t)$, the input current $i(t) = I(t) + \tilde{i}(t)$, the output voltage $v(t) = V + \tilde{v}(t)$, the voltage control action $u(t) = U + \tilde{u}(t)$, and the input voltage $v_s(t) = V_s(t) + \tilde{v}_s(t)$ are replaced in (6), where the capitalized variables are steady-state functions and the perturbation signals are denoted by ˜ sign.

Additionally, the nominal steady-state averaged input voltage stands over one switching period T_s (2) and can be expressed by

$$\begin{aligned} V_s(t) &= \sqrt{2}V_{\rm RMS}[\epsilon_1 \sin(\omega_1 t) + \epsilon_2 \cos(\omega_1 t)] \\ \epsilon_1 &= \frac{(\cos(\omega_1 T_s) - 1)}{\omega_1 T_s} \\ \epsilon_2 &= \frac{\sin(\omega_1 T_s)}{\omega_1 T_s}. \end{aligned} \tag{7}$$

Replacing the averaged steady-state functions and simplifying the quadratic and nonlinear terms of perturbation signals in (6), the following LTP state-space equation can be obtained:

$$\begin{bmatrix} \dot{\tilde{x}}_i(t) \\ \dot{\tilde{i}}(t) \\ \dot{\tilde{v}}(t) \end{bmatrix} = \begin{bmatrix} A_i & -B_i H_i & 0 \\ \dfrac{-2VC_i}{L} & \dfrac{2VD_i Hi}{L} & \gamma_1(t) \\ \gamma_2(t) & \gamma_3(t) & \dfrac{-1}{RC} \end{bmatrix} \begin{bmatrix} \tilde{x_i}(t) \\ \tilde{i}(t) \\ \tilde{v}(t) \end{bmatrix} + \begin{bmatrix} \gamma_4(t) & \dfrac{V^2 B_i H_i}{RV_{\rm RMS}} & 0 \\ \gamma_5(t) & \dfrac{1}{L}\left(1 - \dfrac{2V^3 D_i H_i}{RV_{\rm RMS}}\right) & 0 \\ \gamma_6(t) & \gamma_7(t) & 1 \end{bmatrix} \begin{bmatrix} \tilde{u}(t) \\ \tilde{v}_s(t) \\ \gamma_8(t) \end{bmatrix} \tag{8}$$

where time-varying coefficients $\gamma_n(t)$ are strictly periodic and are given by

$$\begin{aligned} \gamma_1(t) &= \delta_1 \sin(\omega_1 t) + \lambda_1 \cos(\omega_1 t) \\ \delta_1 &= \frac{-1}{L}\left(\frac{\sqrt{2}\omega_1 LV}{RV_{\rm RMS}}\epsilon_2 + \frac{\sqrt{2}V_{\rm RMS}}{V}\epsilon_1\right) \\ \lambda_1 &= \frac{1}{L}\left(\frac{\sqrt{2}\omega_1 LV}{RV_{\rm RMS}}\epsilon_1 - \frac{\sqrt{2}V_{\rm RMS}}{V}\epsilon_2\right) \end{aligned} \tag{9}$$

$$\begin{aligned} \gamma_2(t) &= \delta_2(\epsilon_1 \sin(\omega_1 t) + \epsilon_2 \cos(\omega_1 t)) \\ \delta_2 &= \frac{2\sqrt{2}C_i V^2}{RCV_{\rm RMS}} \end{aligned} \tag{10}$$

$$\begin{aligned} \gamma_3(t) &= \delta_3 \sin(\omega_1 t) + \lambda_3 \cos(\omega_1 t) \\ \delta_3 &= \frac{-1}{C}\left(\frac{-\sqrt{2}\omega_1 LV}{RV_{\rm RMS}}\epsilon_2 - \frac{\sqrt{2}V_{\rm RMS}}{V}\epsilon_1 + \frac{2\sqrt{2}D_i H_i V^2}{RV_{\rm RMS}}\epsilon_1\right) \\ \lambda_3 &= \frac{-1}{C}\left(\frac{\sqrt{2}\omega_1 LV}{RV_{\rm RMS}}\epsilon_1 - \frac{\sqrt{2}V_{\rm RMS}}{V}\epsilon_2 + \frac{2\sqrt{2}D_i H_i V^2}{RV_{\rm RMS}}\epsilon_2\right) \end{aligned} \tag{11}$$

$$\begin{aligned} \gamma_4(t) &= \delta_4(\epsilon_1 \sin(\omega_1 t) + \epsilon_2 \cos(\omega_1 t)) \\ \delta_4 &= \sqrt{2}B_i K V_{\rm RMS} \end{aligned} \tag{12}$$

$$\begin{aligned} \gamma_5(t) &= \delta_5(\epsilon_1 \sin(\omega_1 t) + \epsilon_2 \cos(\omega_1 t)) \\ \delta_5 &= \frac{-2\sqrt{2}D_i VKV_{\rm RMS}}{L} \end{aligned} \tag{13}$$

$$\begin{aligned} \gamma_6(t) &= k_6 + \delta_6 \sin(2\omega_1 t) + \lambda_6 \cos(2\omega_1 t) \\ k_6 &= \frac{2D_i KV^2}{RC}(\epsilon_1^2 + \epsilon_2^2) \\ \delta_6 &= \frac{2\sqrt{2}D_i KV^2}{RCV_{\rm RMS}}\epsilon_1\epsilon_2 \\ \lambda_6 &= \frac{2D_i KV^2}{RC}(\epsilon_2^2 - \epsilon_1^2) \end{aligned} \tag{14}$$

$$\begin{aligned} \gamma_7(t) &= \delta_7(\epsilon_1 \sin(\omega_1 t) + \epsilon_2 \cos(\omega_1 t)) \\ \delta_7 &= \frac{2\sqrt{2}D_i H_i V^4}{CR^2 V_{\rm RMS}^3} \end{aligned} \tag{15}$$

$$\begin{aligned} \gamma_8(t) &= k_8 + \delta_8 \sin(2\omega_1 t) + \lambda_8 \cos(2\omega_1 t) \\ k_8 &= \frac{V}{RC}(\epsilon_1^2 + \epsilon_2^2 - 1) \\ \delta_8 &= \frac{1}{C}\left(\frac{\omega_1 LV^3}{R^2 V_{\rm RMS}^2}(\epsilon_2^2 - \epsilon_1^2) + \frac{2V}{R}\epsilon_1\epsilon_2\right) \\ \lambda_8 &= \frac{1}{C}\left(\frac{-2\omega_1 LV^3}{R^2 V_{\rm RMS}^2}\epsilon_1\epsilon_2 + \frac{V}{R}(\epsilon_2^2 - \epsilon_1^2)\right). \end{aligned} \tag{16}$$

B. Simplified Open-Loop LTP Small-Signal Model

Most of the design techniques assume that the current loop is designed with a bandwidth ten times faster or more than the bandwidth of the voltage loop. This dynamically decouples current and voltage control loops, with makes possible to independently design both controllers. Additionally, to ensure the PFC issue, a sinusoidal internal model is normally added to the current loop to track as close as possible the current reference. Under this assumption, for the voltage loop, the current can be considered as

$$i(t) = \frac{1}{H_i} i^*(t) = \frac{K}{H_i} v_s(t) u(t). \tag{17}$$

In addition, the current state i from (3) may be used to determine the duty cycle for the voltage state v, given by

$$d(t) = \frac{1}{2} + \frac{v_s(t)}{2v(t)} - \frac{L\dot{i}(t)}{2v(t)}. \tag{18}$$

Whether current and voltage control loops are dynamically decoupled, then normally a higher switching frequency is also applied. Since the switching frequency is 40 times higher than the fundamental input voltage frequency ($\frac{\omega_s}{\omega_1} \geq 40$), the angular coefficients of the averaged input voltage (7) may be approximated by the first-order Taylor series, resulting in $\sin(\omega_1 T_s) \approx \omega_1 T_s$ and $\cos(\omega_1 T_s) \approx 1$. In terms of simplification of the state-space model in (27), this condition reduces its periodic coefficients, where $\epsilon_1 = 0$ and $\epsilon_2 = 1$, and can be applied directly. Furthermore, this condition simplifies the averaged input voltage, which results in

$$V_s(t) = \sqrt{2} V_{\mathrm{RMS}} \cos(\omega_1 t). \tag{19}$$

Thus, substituting (17) and (18) into the voltage equation $\dot{v}(t)$ (3) results in the following nonlinear expression:

$$v(t)\dot{v}(t) = \frac{-1}{RC} v^2(t) + \frac{1}{C} v_s(t) i(t) - L\dot{i}(t) i(t). \tag{20}$$

Then, applying the perturbation signal around the steady-state condition and simplifying the second-order and nonlinear terms of perturbation result in the following simplified LTP model:

$$\dot{\tilde{v}}(t) = \frac{-2}{RC}\tilde{v}(t) + \begin{bmatrix} \phi_1 & \phi_2 & 1 \end{bmatrix} \begin{bmatrix} \tilde{u}(t) \\ \tilde{v}_s(t) \\ \phi_3(t) \end{bmatrix} \tag{21}$$

in which time-varying coefficients are

$$\phi_1(t) = \frac{K V_{\mathrm{RMS}}^2}{H_i V C} + \frac{K V_{\mathrm{RMS}}^2}{H_i V C} \cos(2\omega_1 t) + \frac{2LVK\omega_1}{H_i RC} \sin(2\omega_1 t) \tag{22}$$

$$\phi_2(t) = \frac{2\sqrt{2}V}{RCV_{\mathrm{RMS}}} \cos(\omega_1 t) + \frac{\sqrt{2}LV^3\omega_1}{R^2 C V_{\mathrm{RMS}}^3} \sin(\omega_1 t) \tag{23}$$

$$\phi_3(t) = \frac{V}{RC} \cos(2\omega_1 t) + \frac{LV^3\omega_1}{R^2 C V_{\mathrm{RMS}}^2} \sin(2\omega_1 t). \tag{24}$$

The first-order model (21) shows the voltage behavior $\tilde{v}$ for the control action $\tilde{u}$ and for input voltage disturbance $\tilde{v}_s$. The additional input ϕ_3 represents the oscillation of the dc link under the nominal steady-state condition.

One can observe from the ac–dc full-bridge converter output voltage model given in (21) that for a constant input u, an output voltage v is obtained, which is comprised of a dc component with a voltage ripple of frequency $2\omega_1$, which is represented in (21) by complex exponential terms. The origin of an output harmonic of frequency $2\omega_1$ when a dc input is applied is named frequency shifting.

The LTI model that relates the control action disturbance $\tilde{u}$ to the output voltage $\tilde{v}$ can be directly determined from (21) disregarding its sinusoidal terms, which results in the following:

$$\dot{\tilde{v}}(t) = \frac{-2}{RC}\tilde{v}(t) + \frac{K V_{\mathrm{RMS}}^2}{H_i V C}\tilde{u}(t) \tag{25}$$

in which the well-known TF is expressed by

$$G_v(s) = \frac{\tilde{V}(s)}{\tilde{U}(s)} = \left(\frac{K V_{\mathrm{RMS}}^2}{H_i V C}\right) \frac{1}{s + \frac{2}{RC}}. \tag{26}$$

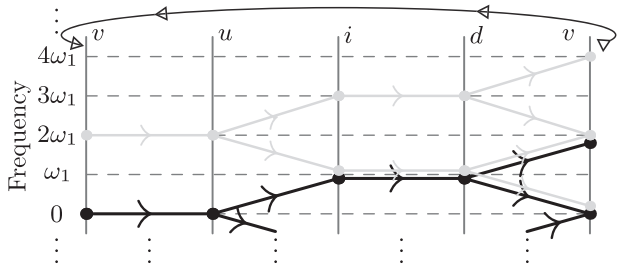

Fig. 2. Converter frequency mapping behavior for source voltage frequency ω_1 and system variables: voltage control action u, inductor current reference i^*, duty cycle d, and dc-link voltage v.

The LTI model well represents the converter's dynamics when the capacitance C is large and the voltage control loop presents a low-pass characteristic, which results in significant attenuation of the components of v with frequencies $2\omega_1$ and higher. Since these conditions are normally ensured in most of the ac–dc full-bridge converters, the techniques of analysis and design of this converter, based on the TF given in (26), have been appropriate in most of the cases. However, when these conditions are not ensured, these techniques may fail. In this case, another system theory that includes the converter's frequency shifting behavior described in this section must be considered.

For better understanding of the impact of frequency shifting on the control signals, Fig. 2 presents the frequency signal mapping, supposing that the full bridge is in closed loop, by a voltage controller, not included in the model. The vertical axis presents the positive-harmonic components of the fundamental frequency ω_1, while the horizontal axis presents the fundamental nodes of the control loop. Since the signals are fed back by the control system, the horizontal axis should be repeated indefinitely. First, the black line in Fig. 2 is analyzed, where it is assumed *a priori* that the output voltage v is constant. Since the controller C_v is linear, voltage error e_v and control action u are also constant. As a result of the product of u and sinusoidal signal Kv_s, the input current i is a sinusoidal waveform with frequency ω_1. Based on that, due to the intrinsic converter operation, there is a product of i and the sinusoidal duty cycle d, which results in the dc-link voltage v. The product of two sinusoidal waveforms results in v with a dc component plus a sinusoidal component with frequency $2\omega_1$. Since both components are fed back, one can observe now two frequency mappings represented in Fig. 2: the black one, which represents the path of dc component, and the gray one, which represents the path of the component of frequency $2\omega_1$. Extending this frequency shifting for all output components results in infinite terms of harmonic interactions.

III. Review of Systems With Frequency Shifting and Stability

The continuous LTP system theory is suitable to describe and analyze the behavior of dynamic systems with frequency shifting. In this approach, the sinusoidal terms of (21) are replaced by its complex exponential form and, then, are included into dynamic matrices A, B, C, and D in the open-loop state-space

time-domain representation, given by

$$\dot{x}(t) = A(t)x(t) + B(t)u(t)$$
$$y(t) = C(t)x(t) + D(t)u(t) \tag{27}$$

where $A(t)$, $B(t)$, $C(t)$, and $D(t)$ are strictly periodic matrices with period T_1.

The LTP analysis and synthesis has been a focus for a long time. In particular, the stability analysis is much harder than of LTI systems. The classical Floquet analysis of LTP systems has been widely used in many areas to address this issue [34]–[36]. However, the Floquet theorem only presents a methodology for the closed-loop analysis and only provides the z-plane location of its monodromy matrix eigenvalues. Although an alternative numerical procedure has been developed to provide open-loop analysis, based on the Floquet theory, it only results in a yes or no answer to the question of stability. Thus, the Floquet theory can only serve as an analysis tool, and not as a compensator synthesis tool [22].

In the other way, the HTF is a linear operator that relates all of the input harmonics to all of the output harmonics in a systematic way analogous to TF in LTI systems. The HTF is the Laplace frequency-domain representation of the LTP system and is always a multiple-input multiple-output LTI representation of the LTP plant (27).

Basically, since the input and the output are written as vectors of their harmonic components in the frequency domain, then the frequency modulation matrix $\mathcal{N}$ and the Toeplitz transformation $\{\mathcal{A},\ \mathcal{B},\ \mathcal{C},\ \mathcal{D}\}$ of $\{A(t), B(t), C(t), D(t)\}$ [37] may form a multivariable LTI system, named harmonic state space [18], [22], [38]

$$s\mathcal{X}(s) = (\mathcal{A} - \mathcal{N})\mathcal{X}(s) + \mathcal{B}\mathcal{U}(s)$$
$$\mathcal{Y}(s) = \mathcal{C}\mathcal{X}(s) + \mathcal{D}\mathcal{U}(s) \tag{28}$$

which is equivalent to an open-loop LTP model. The HTF from (28) is given by

$$\boldsymbol{G} = \mathcal{C}\left[sI - (\mathcal{A} - \mathcal{N})\right]^{-1}\mathcal{B} + \mathcal{D}. \tag{29}$$

The closed-loop system stability may be checked by inspecting the eigenloci of the following open-loop system:

$$\boldsymbol{T}(s) = \boldsymbol{C}(s)\boldsymbol{G}(s)\boldsymbol{H}(s) \tag{30}$$

by applying the generalized Nyquist stability criterion, where $\boldsymbol{C}(s)$ is the HTF form of the controller and $\boldsymbol{H}(s)$ is the sensor HTF form. If the sensor is a simple gain, then $\boldsymbol{H}(s)$ may be a constant [29], [39].

The stability criteria are evaluated in a similar manner to that of the single-input single-output (SISO) system but considering all eigenlocus contours [29]. Eigenlocus is the plot of all eigenvalues in the complex plane calculated for the Nyquist contour [39]. Since LTP systems have the folding effect, the Nyquist path is simplified, as shown in Fig. 3.

Furthermore, since the eigenlocus is the open-loop frequency response, the gain margin (GM) and phase margin (PM) interpretations based on the eigenlocus are identical to those in LTI systems. These are useful indicators for use as a control design tool. Since the system has several eigenloci, the GM and the PM

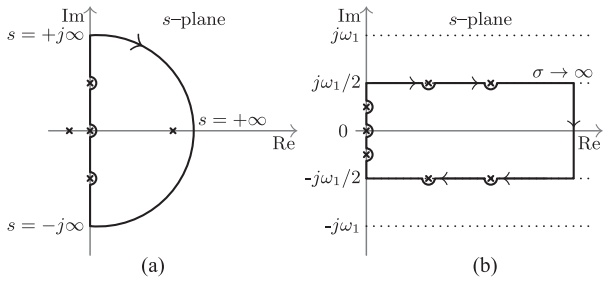

Fig. 3. Modified Nyquist contours. (a) LTI Nyquist path $\mathcal{C}_{\text{LTI}}$. (b) LTP Nyquist path $\mathcal{C}_{\text{LTP}}$.

TABLE I
CONVERTER PARAMETERS AND NOMINAL SPECIFICATION

Description	Parameter
Nominal input voltage	$V_{\text{RMS}} = 127$ V
Input frequency	$\omega_1 = 2\pi 60$ rad/s
Output voltage	$V = 300$ V
Nominal output power	$P_o = 375$ W
Input inductor	$L = 560\ \mu$H
DC capacitor	$C = 680\ \mu$F
Load resistance	$R = 240\ \Omega$
Switching/Sampling frequency	$T_s = 46875$ Hz
Direct input voltage gain	$K = 1/(127\sqrt{2})$ A/V
Feedback voltage gain	$H_v = 1$
Feedback current gain	$H_i = 1$

are defined as the minimum value among them. More detailed issues about the HTF can be found in [22] and [23]. The Bode frequency response has been shown in some works [40], [41], but we choose the Nyquist diagram as the analysis tool.

IV. STABILITY ANALYSIS OF AC–DC FULL-BRIDGE CONVERTERS: A COMPARISON BETWEEN LTI AND LTP APPROACHES

This section presents a comparison of stability analysis considering LTI and LTP approaches of the dc-link voltage controller for the ac–dc full-bridge converter with reduced dc-link capacitance. In order to obtain a controller with fast dynamic response without compromising the sinusoidal waveform of the input current, notch filters were designed and tuned at $2\omega_1$ to mitigate this frequency component feedback in the control loop [12], [42]. The controllers were designed by using classical SISO methods considering the LTI model presented in (26).

The converter parameters considered in this analysis are shown in Table I. Both current and voltage controllers were designed by employing LTI-averaged models shown in Table II. The inner current control loop was designed to be more than ten times faster than the voltage loop. As a result, both loops are dynamically decoupled, and the inner current loop can be considered a gain $1/H_i$ for outer voltage loop control analysis. A notch filter with 60-dB attenuation at frequency 120 Hz was included in the voltage controller to avoid PF deterioration [12]. The resulting controllers are shown in Table II.

TABLE II
CONTROL PARAMETERS

Description	Transfer Function
LTI current model	$G_i(s) = \frac{-1.071(10)^6}{s}$
LTI voltage model	$G_v(s) = \frac{440.2}{s+6.127}$
Current compensator	$C_i(s) = \frac{-1800\left(s+2\pi(10)^3\right)}{s(s+2\pi 15(10)^3)}$
Voltage compensator	$C_v(s) = C_n(s)C_f(s)$, where $C_n(s) = \frac{s^2+4\zeta\omega_1 s+(2\omega_1)^2}{(s+2\omega_1)^2}, \zeta = 10^{-3}$ $C_f(s) = \frac{4604(s+2\pi(3))}{s(s+2\pi(500))}$

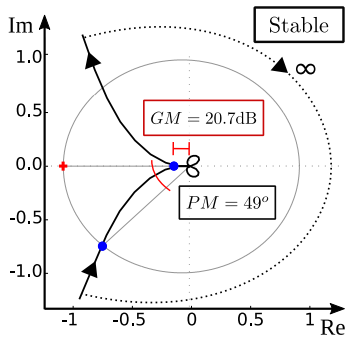

Fig. 4. Nyquist diagram for the outer voltage loop represented by the LTI model.

A. Stability Analysis: The LTI Case

The LTI stability analysis approach is used when the converter is represented by the average LTI model described in (26). The stability analysis in the frequency domain has been done using the Nyquist criterion represented in Fig. 4, which is the eigenlocus contour of the open-loop equation $H_v C_v(s) G_v(s)$ calculated for the path shown in Fig. 3(a). The graphical interpretation indicates a stable closed-loop behavior, because the eigenlocus contour does not encircles the point $(-1+j0)$. The calculated GM $= 10.84 = 20.7$ dB @ $2\pi 98$ rad/s and the PM $= 49°$ @ $2\pi 38$ rad/s.

B. Stability Analysis: The LTP Case

The LTP stability analysis approach is used when the converter is represented by the HTF model described in (30). In order to obtain the HTF representation of the system, the converter model (21) may be represented by state-space equations (27), for output $y(t) = \tilde{v}(t)$, input $u(t) = \tilde{u}(t)$, and $T_1 = \frac{2\pi}{\omega_1}$, whose matrices $A(t)$, $B(t)$, $C(t)$, and $D(t)$ should be separated into their Fourier coefficients, substituting the sinusoidal terms into their exponential form, that are given by [43]

$$A(t) = -\frac{2}{RC}$$
$$B(t) = B_{-2}\,\mathrm{e}^{-j2\omega_1 t} + B_0 + B_2\,\mathrm{e}^{j2\omega_1 t} \tag{31}$$
$$= \left(\frac{b_1}{2} + \frac{jb_2}{2}\right) e^{-j2\omega_1 t} + b_0 + \left(\frac{b_1}{2} - \frac{jb_2}{2}\right) e^{j2\omega_1 t} \tag{32}$$
$$C(t) = 1 \quad \text{and} \quad D(t) = 0 \tag{33}$$

where the coefficients $b_0 = b_1 = \frac{KV_{\mathrm{RMS}}^2}{H_i V C}$ and $b_2 = \frac{2LVK\omega_1}{H_i RC}$ are derived from ϕ_1 in (22).

One can observe that all matrices have null coefficients for harmonics excepting $B(t)$, which has the second-harmonic terms. In this way, the following Toeplitz matrices are obtained:

$$\mathcal{A} = -\frac{2}{RC}\,\mathcal{I} \qquad \mathcal{C} = \mathcal{I} \qquad \mathcal{D} = 0\mathcal{I} \tag{34}$$

$$\mathcal{B} = \begin{bmatrix} \ddots & \ddots & \ddots & \ddots & \ddots & \ddots & \ddots \\ \ddots & B_0 & 0 & B_{-2} & 0 & 0 & \ddots \\ \ddots & 0 & B_0 & 0 & B_{-2} & 0 & \ddots \\ \ddots & B_2 & 0 & B_0 & 0 & B_{-2} & \ddots \\ \ddots & 0 & B_2 & 0 & B_0 & 0 & \ddots \\ \ddots & 0 & 0 & B_2 & 0 & B_0 & \ddots \\ \ddots & \ddots & \ddots & \ddots & \ddots & \ddots & \ddots \end{bmatrix} \tag{35}$$

where $\mathcal{I}$ is an identity matrix with doubly-infinite dimension. Note that Toeplitz matrices $\mathcal{A}$, $\mathcal{C}$, and $\mathcal{D}$ have diagonal form since the LTP model has unity dimension. On the other hand, $\mathcal{B}$ is expanded by its harmonic coefficients.

Thus, the final HTF model of the plant is obtained by solving (29) using the Toeplitz matrices (34) and (35)

$$\boldsymbol{G_v}(s) = \begin{bmatrix} \ddots & \ddots & \ddots & \ddots & \ddots \\ \ddots & \frac{B_0}{s+\frac{2}{RC}-j\omega_1} & 0 & \frac{B_{-2}}{s+\frac{2}{RC}-j\omega_1} & \ddots \\ \ddots & 0 & \frac{B_0}{s+\frac{2}{RC}} & 0 & \ddots \\ \ddots & \frac{B_2}{s+\frac{2}{RC}+j\omega_1} & 0 & \frac{B_0}{s+\frac{2}{RC}+j\omega_1} & \ddots \\ \ddots & \ddots & \ddots & \ddots & \ddots \end{bmatrix}. \tag{36}$$

The LTP stability was graphically analyzed based on the Nyquist plot of the open-loop HTF eigenlocus contours of $H_v \boldsymbol{C}_v(s)\boldsymbol{G}_v(s)$, where $\boldsymbol{C}_v(s)$ is the controller HTF matrix obtained through the controller $C_v(s)$. The computational realization considered a truncated HTF matrix limited to the fourth-harmonic component, and the right-half-plane (RHP) frequency was restricted to $\sigma = 10^3 \mathrm{rad/s}$. In this result, the truncation were defined for values that when increase do not cause changes in the analysis. These simplifications were carefully chosen

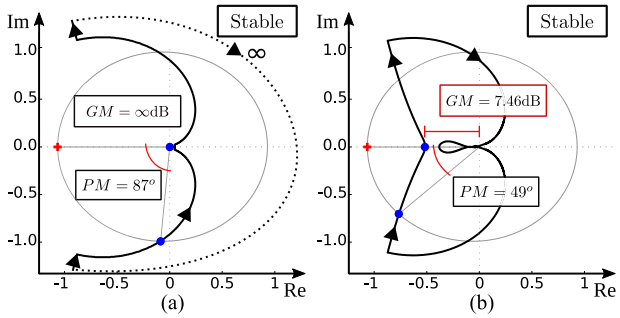

Fig. 5. Nyquist diagrams for the outer voltage loop represented by the LTP model. (a) Eigenlocus contour of λ_1. (b) Eigenlocus contour of λ_2.

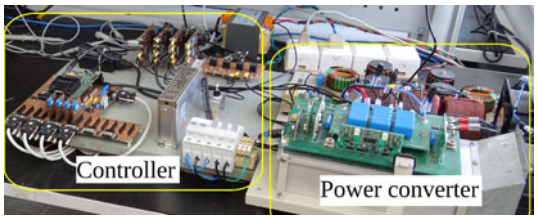

Fig. 6. Experimental setup.

because they may affect the accuracy of the stability analysis. Fig. 5(a) and (b) represents the contour plots for the two more representative eigenloci, while the plots of the other seven few significant eigenlocus contours keep around the origin and are not presented.

According to the generalized Nyquist theorem [29], the closed loop is stable if and only if the eigenlocus encircles $(-1 + j0)$ (Z) in the same number as the open-loop RHP poles (P), given by $N = Z - P = 0$. The open-loop TF $H_v \boldsymbol{C}_v(s)\boldsymbol{G}_v(s)$ has no poles inside the RHP fundamental strip enclosed by the Nyquist path, so $P = 0$. Therefore, the closed-loop control system is stable if and only if the composition of all eigenloci does not encircle the point $(-1 + j0)$, i.e., $Z = 0$. From the Nyquist plots of Fig. 5(a) and (b), one can observe that the point $(-1 + j0)$ is not encircled by any eigenlocus contour; hence, the closed-loop system is stable for the nominal condition.

One of the main advantages of the Wereley approach is that the GM and the PM may be performed in a similar way to the Nyquist LTI methodology. Therefore, the resulting GM, obtained in Fig. 5(b), is GM $= 2.36 = 7.46$ dB, which is 4.60 times smaller than the one obtained through the LTI model in Fig. 4. On the other hand, the minimum PM is similar than the one obtained from the LTI approach (PM $= 49°$).

C. Experimental Validation

Experimental results of the ac–dc full-bridge converter have been carried out for validation of both approaches presented in previous section. The experimental setup is illustrated in Fig. 6, for which parameters are presented in Table I. The controller is a 32-bit floating-point digital processor, 150-MHz clock. The digital controller realization is performed, instead analogical, since the controller response has to be ensured. In this way, the

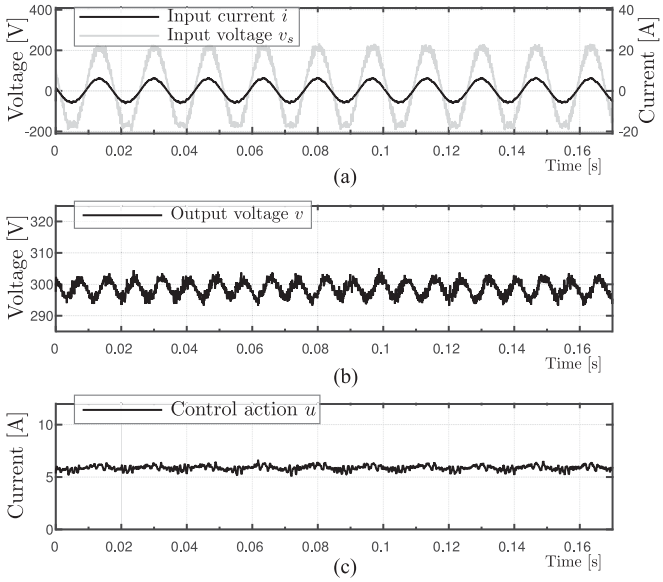

Fig. 7. Experimental results for the nominal case.

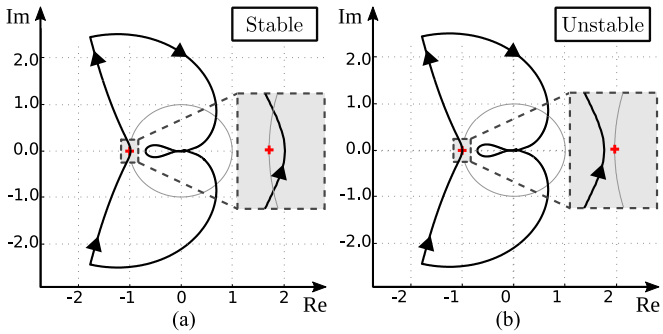

Fig. 8. Eigenlocus contour of λ_2 from LTP stability analysis for different values of β. (a) $\beta = 2.34$. (b) $\beta = 2.38$.

controller parameters that cause instability can be more exactly determined. To preserve the controller response on discretization, a high sampling frequency of 46 875 kHz is adopted to reduce the zero-order-hold influence on the controller response. Thus, the digital and the continuous response are close enough to approximate them as the same, since the methodology is applied in continuous time.

Fig. 7 shows the experimental results for the nominal system presented previously. In this case, the system is closed-loop stable in both approaches. Fig. 7(a) shows the input voltage and the input current. One can observe the dominant sinusoidal behavior and the small phase shift between waveforms. Fig. 7(b) shows the dc-link voltage, where one can observe the 120-Hz ac component in addition to the dc voltage. Fig. 7(c) shows the reference for the magnitude of input current, which is the control action for the outer voltage plant.

For evaluation of the stability analysis accuracy under different approaches, a gain β in series was intentionally inserted with the controller $\boldsymbol{C}_v(s)$. The stability limit was evaluated from the LTP approach, given that GM $= 7.46$ dB in this case, which is lower than GM $= 20.7$ dB from the LTI approach.

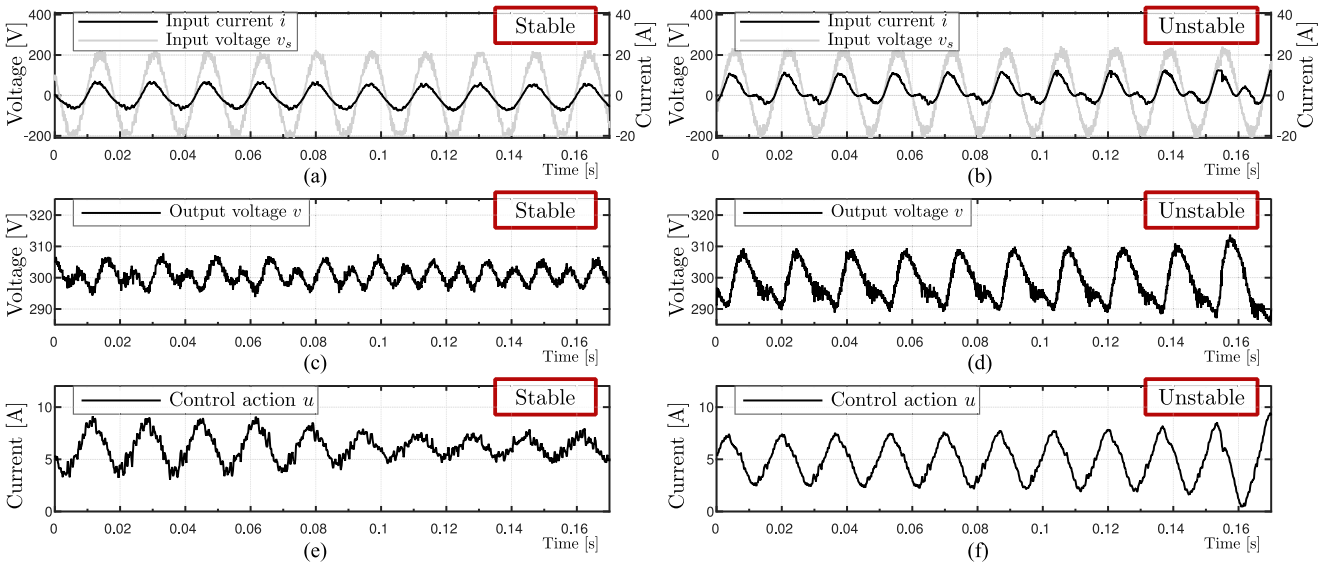

Fig. 9. Experimental results. Left column: $\beta = 2.20$. Right column: $\beta = 2.21$.

Both LTP analysis and experimental results were performed around the stability limits aiming to compare its results. For the LTP analysis, the most important eigenlocus is λ_2; only this eigenvalue is presented for the stability limit analysis. In this way, Fig. 8(a) presents the eigenlocus contour of λ_2 for $\beta = 2.34$. In this case, no eigenlocus contour encircles $(-1 + j0)$; hence, the system is closed-loop stable. However, this eigenlocus contour crosses the real negative axis close to $(-1 + j0)$, which means the GM is almost zero. On the other hand, Fig. 8(b) shows the eigenlocus contour of λ_2 for $\beta = 2.38$. In this case, the eigenlocus contour encircles the point $(-1 + j0)$, which results in an unstable case.

The stability limit was determined experimentally by varying the gain β until achieving its instability. Therefore, the left column of Fig. 9 presents a transient result for a stable condition with $\beta = 2.20$, while the right column of Fig. 9 shows an unstable case with $\beta = 2.21$. One can realize the stable condition easily by observing the convergence of the control action signal in Fig. 9(e). On the other hand, the unstable behavior can be observed in Fig. 9(b), (d), and (f), since it presents a divergent shape.

Therefore, the experimental results demonstrate that the LTP method can precisely determine the stability limits of the converter. Experimental results present a gain margin of 2.20. Compared to those, the LTP presents a GM = 2.36 (7.46 dB), only 7% higher. On the other hand, when the conventional LTI approach is compared to the same experimental results, the gain margin achieved is 10.84 (20.7 dB), which means an increase of 4.9 times. It worth mentioning that this difference is totally dependent on the open-loop design condition.

V. Impact of Parameters Variations on Closed-Loop Stability of the AC–DC Converter

From the analysis presented in previous sections, one can conclude that the LTP approach leads to accurate stability criteria. On the other hand, the LTI approach may be inappropriate in cases of reduced capacitance or the dynamic of the control loop is faster than usual. However, design techniques of ac–dc full-bridge converters based on LTI models have been successfully used for decades, since most of the design constraints are not so restrictive as considered in the design presented in this paper. Therefore, it is important to find out under which conditions the LTI analysis is suitable and when it is not.

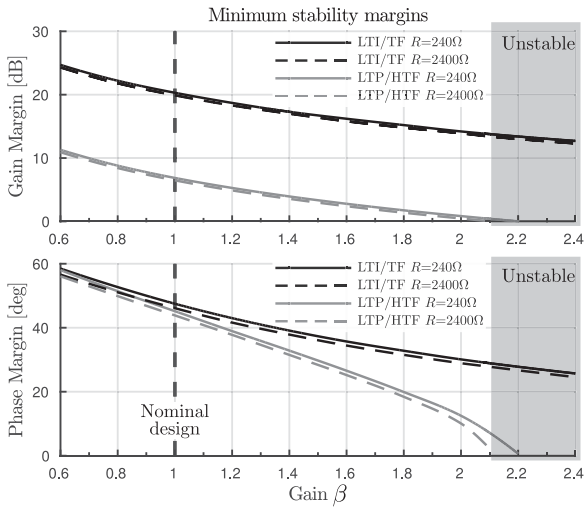

Fig. 10. GM and PM of the ac–dc full-bridge converter for different values of gain β and $C = 680\ \mu$F.

Assuming the converter and controller presented in Section IV, Figs. 10 and 11 show the impact of modification of a single system parameter on the GM and the PM of the outer voltage loop. It worth mentioning that this parameter investigation was performed using the theoretical analysis. In this way, it can be observed that the GM, according the LTI approach, is 13 dB higher than the LTP approach in all cases. This difference

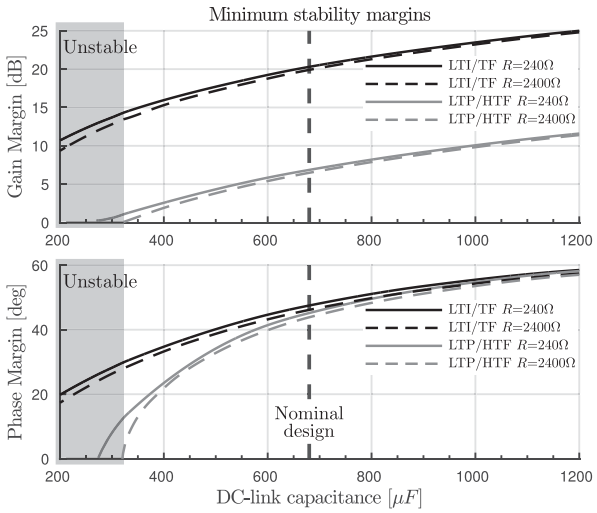

Fig. 11. GM and PM of the ac–dc full-bridge converter for different values of dc-link capacitance C and $\beta = 1$.

is due to an eigenlocus in LTP that does not have a counterpart in the LTI analysis.

Fig. 10 shows the variation of series gain β for nominal resistive load ($R = 240\ \Omega$) and for 10% of the resistive nominal load ($R = 2400\ \Omega$). One can observe that the PM is similar for $\beta < 1$, but it is significantly different for $\beta > 1$. As shown in Section IV, the LTP system becomes unstable for $\beta = 2.2$, but the LTI system presents GM ≈ 10.84.

Fig. 11 presents a similar analysis for variation of dc-link capacitance C. For $C \geq 600\ \mu$F, both LTI and LTP approaches result in a similar PM. However, for $C \leq 600\ \mu$F, one can observe that the PM according to the LTP analysis drops significantly to zero at $C \approx 275\ \mu$F. However, for this value of C, the LTI approach results in PM $\approx 25°$, which is significantly different.

In both figures, one can observe that both the GM and the PM do not change significantly from nominal load to light load. One reason why these performance indexes do not change significantly is the strong attenuation of the resonance peak by the notch filter, even for light loads.

Finally, one can observe that the central component $\boldsymbol{G}_{v[0,0]}(s)$ in (36) is the TF that relates the dc input level $U_0(s)$ to the dc output component $Y_0(s)$. This $\boldsymbol{G}_{v[0,0]}(s)$ matches the LTI-averaged model of the converter $G_v(s)$ given in (26). Consequently, one can conclude that for cases where the feedback of harmonics components is not significant, the components of higher order of $\boldsymbol{G}_v(s)$ have a reduced impact on the system stability. Under this condition, the stability analysis from both the LTI or LTP approaches leads to similar results. However, when the converter presents a reduced dc-link capacitance or a high-frequency outer voltage loop bandwidth, the use of the LTP approach may be required to correctly design the voltage controller.

VI. Conclusion

In this study, it was demonstrated that the stability of the dc-link outer voltage loop of PFC ac–dc converters may not be always well stated by conventional LTI models. On the other hand, it was shown that LTP models better represent the converter's dynamics since they include the converter sinusoidal modulation and harmonic interactions. In this approach, the dc-link voltage ripple due to sinusoidal modulation is no longer disregarded, because the sinusoidal multiplications are included in the model. The LTP approach is recommended if the dc-link voltage ripple is high or a high-bandwidth dc-link voltage control is designed.

The results we have presented may assist in the design of the control system of PFC ac–dc converters when small dc-link capacitance is used or a fast voltage dynamic response is necessary. This is important to increase the lifetime and enhance the performance of these converters.

Acknowledgment

The authors would like to thank the anonymous reviewers for their valuable comments and suggestions to improve an original version of this manuscript.

References

[1] P. Alemi, Y.-C. Jeung, and D.-C. Lee, "DC-link capacitance minimization in T-type three-level AC/DC/AC PWM converters," *IEEE Trans. Ind. Electron.*, vol. 62, no. 3, pp. 1382–1391, Mar. 2015.

[2] S. Dusmez and A. Khaligh, "Generalized technique of compensating low-frequency component of load current with a parallel bidirectional DC/DC converter," *IEEE Trans. Power Electron.*, vol. 29, no. 11, pp. 5892–5904, Nov. 2014.

[3] X. Cao, Q.-C. Zhong, and W.-L. Ming, "Ripple eliminator to smooth dc-bus voltage and reduce the total capacitance required," *IEEE Trans. Ind. Electron.*, vol. 62, no. 4, pp. 2224–2235, Apr. 2015.

[4] Y. Hu, Y. Du, W. Xiao, S. Finney, and Wenping,"DC-link voltage control strategy for reducing capacitance and total harmonic distortion in single-phase grid-connected photovoltaic inverters," *IET Power Electron.*, vol. 8, no. 8, pp. 1386–1393, 2015.

[5] W.-J. Lee and S.-K. Sul, "DC-link voltage stabilization for reduced dc-link capacitor inverter," *IEEE Trans. Ind. Appl.*, vol. 50, no. 1, pp. 404–414, Jan. 2014.

[6] B. Wang, X. Ruan, K. Yao, and M. Xu, "A method of reducing the peak-to-average ratio of led current for electrolytic capacitor-less ac-dc drivers," *IEEE Trans. Power Electron*, vol. 25, no. 3, pp. 592–601, Mar. 2010.

[7] A. Prodic, J. Chen, D. Maksimovic, and R. W. Erickson, "Self-tuning digitally controlled low-harmonic rectifier having fast dynamic response," *IEEE Trans. Power Electron.*, vol. 18, no. 1, pp. 420–428, Jan. 2003.

[8] S. Wall and R. Jackson, "Fast controller design for single-phase power-factor correction systems," *IEEE Trans. Ind. Electron.*, vol. 44, no. 5, pp. 654–660, Oct. 1997.

[9] R. Ghosh and G. Narayanan, "A simple method to improve the dynamic response of single-phase PWM rectifiers," *IEEE Trans. Ind. Electron.*, vol. 55, no. 10, pp. 3627–3634, Oct. 2008.

[10] Z. Yang and C. Paresh, "A novel technique to achieve unity power factor and fact transient response in ac-to-dc converters," *IEEE Trans. Power Electron.*, vol. 16, no. 6, pp. 764–775, Nov. 2001.

[11] D. Lamar, A. Fernandez, M. Arias, M. Rodriguez, J. Sebastian, and M. Hernando, "A unity power factor correction preregulator with fast dynamic response based on a low-cost microcontroller," *IEEE Trans. Power Electron.*, vol. 23, no. 2, pp. 635–642, Mar. 2008.

[12] L. Nodari, M. Mezaroba, L. Michels, and C. Rech, "A new digital control system for a single-phase half-bridge rectifier with fast dynamic response," in *Proc. IEEE Energy Convers. Congr. Expo.*, 2010, pp. 1204–1211.

[13] L. V. Belinaso, R. Z. Scapini, and L. Michels, "Modeling and analysis of single phase full-bridge PFC boost rectifier using the LTP approach," in *Proc. Brasilian Power Electron. Conf*, Jul. 2011, pp. 93–100.

[14] R. Z. Scapini, L. V. Bellinaso, and L. Michels, "Is conventional stability analysis based on LTI approach valid for PFC converters?" in *Proc. Power Electron. South Amer.*, São Paulo, Brazil, Sep. 2012, p. 8.

[15] S. Almér and U. Jönsson,"Harmonic analysis of pulse-width modulated systems," *Automatica*, vol. 45, no. 4, pp. 851–862, Apr. 2009.
[16] E. Möllerstedt and B. Bernhardsson, "A harmonic transfer function model for a diode converter train," in *Proc. IEEE Power Eng. Soc. Winter Meeting*, 2000, vol. 2, pp. 957–962.
[17] G. Love and A. Wood, "Harmonic state space model of power electronics," in *Proc. 13th Int. Conf. Harmonics Quality Power*, Oct. 2008, pp. 1–6.
[18] J. R. C. Orillaza and A. R. Wood, "Harmonic state-space model of a controlled TCR," *IEEE Trans. Power Del.*, vol. 28, no. 1, pp. 197–205, Jan. 2013.
[19] Q. Zhong, L. Lin, G. Wang, Y. Zhang, and Z. Wu, "Harmonic analysis model for voltage source converter under unbalanced conditions," *IET Gener., Transmiss. Distrib.*, vol. 9, no. 1, pp. 12–21, 2015.
[20] M. S. Allen, M. W. Sracic, S. Chauhan, and M. H. Hansen, "Output-only modal analysis of linear time-periodic systems with application to wind turbine simulation data," *Mech. Syst. Signal Process.*, vol. 25, no. 4, pp. 1174–1191, 2011.
[21] J. T. B. A. Kessels, J. Sijs, R. M. Hermans, A. A. H. Damen, and P. P. J. van den Bosch, "On-line identification of vehicle fuel consumption for energy and emission management: An LTP system analysis," in *Proc. Amer. Control Conf.*, Jun. 2008, pp. 2070–2075.
[22] N. M. Wereley, "Analysis and control of linear periodically time varying systems," Ph.D. dissertation, Dept. Aeronaut. Astronaut., Massachusetts Inst. Technol., Cambridge, MA, USA, 1990.
[23] E. Möllerstedt, "Dynamic analysis of harmonics in electrical systems," Ph.D. dissertation, , Dept. Autom. Control, Lund Inst. Technol., Lund, Sweden, 2000.
[24] H. Sandberg, E. Möllerstedt, and Bernhardsson, "Frequency-domain analysis of linear time-periodic systems," *IEEE Trans. Autom. Control*, vol. 50, no. 12, pp. 1971–1983, Dec. 2005.
[25] N. M. Wereley and S. R. Hall, "Frequency response of linear time periodic systems," in *Proc. 29th IEEE Conf. Decision Control*, Dec. 1990, vol. 6, pp. 3650–3655.
[26] N. M. Wereley and S. R. Hall, "Linear time periodic systems: Transfer function, poles, transmission zeroes and directional properties," in *Proc. Amer. Control Conf.*, Jun. 1991, vol. 6, pp. 1179–1184.
[27] S. R. Hall and N. M. Wereley, "Generalized Nyquist stability criterion for linear time periodic systems," in *Proc. Amer. Control Conf.*, May 1990, pp. 1518–1525.
[28] B. Strobl, "Analysis of stability for networks including converters," in *Proc. Eur. Conf. Power Electron. Appl.*, Sep. 2007, pp. 1–10.
[29] C. Desoer and Y.-T. Wang, "On the generalized Nyquist stability criterion," *IEEE Trans. Autom. Control*, vol. AC-25, no. 2, pp. 187–196, Apr. 1980.
[30] J. Zhou and T. Hagiwara, "Generalized nyquist criterion of continuous-time periodic systems and its implementation I: Theoretic results," in *Proc. 41st SICE Annu. Conf.*, Aug. 2002, vol. 3, pp. 1700–1705.
[31] R. Costa-Castelló, R. Griñó, and E. Fossas, "Resonant control of a single-phase full-bridge unity power factor boost rectifier," in *Proc. IEEE Int. Conf. Control Appl.*, Oct. 2007, pp. 599–604.
[32] H.-Y. Kanaan and K. Al-Haddad, "Modeling techniques applied to switch-mode power converters: Application to the boost-type single-phase full-bridge rectifier," in *Proc. Conf. Human Syst. Interact.*, 2008, pp. 979–983.
[33] H.-C. Chen and J.-Y. Liao, "Bidirectional current sensorless control for the full-bridge AC/DC converter with considering both inductor resistance and conduction voltages," *IEEE Trans. Power Electron.*, vol. 29, no. 4, pp. 2071–2082, Apr. 2014.
[34] J. Zhou, T. Hagiwara, and M. Araki, "Stability analysis of continuous-time periodic systems via the harmonic analysis," *IEEE Trans. Autom. Control*, vol. 47, no. 2, pp. 292–298, Feb. 2002.
[35] S. Almer and U. T. Jonsson, "Harmonic Lyapunovfunctions in the analysis of periodically switched systems," in *Proc. 45th IEEE Conf. Decision Control*, 2006, pp. 2759–2764.
[36] A. E. Aroudi, M. Orabi, R. Haroun, and L. Martinez-Salamero, "Asymptotic slow-scale stability boundary of PFC ac-dc power converters: Theoretical prediction and experimental validation," *IEEE Trans. Ind. Electron.*, vol. 58, no. 8, pp. 3448–3460, Aug. 2011.
[37] R. M. Gray, *Toeplitz and Circulant Matrices: A Review*, vol. 2. Boston, MAUSA: Now Publishers, 2006.
[38] M. Hwang, B. Das, A. Wood, N. Watson, and Y. Liu, "Experimental validation of the harmonic state-space model of a Graetz bridge converter," *Int. Trans. Elect. Energy Syst.*, vol. 24, no. 9, pp. 1343–1355, 2014.
[39] Y.-P. Tian, *Frequency-Domain Analysis and Design of Distributed Control Systems*. Hoboken, NJ, USA: Wiley, Aug. 2012.
[40] H. Sandberg and B. Bernhardsson, "A bode sensitivity integral for linear time-periodic systems," *IEEE Trans. Autom. Control*, vol. 50, no. 12, pp. 2034–2039, Dec. 2005.
[41] A. Nakhmani, M. Lichtsinder, and E. Zeheb, "Generalized Nyquist criterion and generalized bode diagram for analysis and synthesis of uncertain control systems," in *Proc. IEEE 24th Conv. Elect. Electron. Eng. Israel*, Nov. 2006, pp. 250–254.
[42] A. Prodic, J. Chen, R. W. Erickson, and D. Maksimovic, "Digitally controlled low-harmonic rectifier having fast dynamic responses," in *Proc. 17th Annu. IEEE Appl. Power Electron. Conf. Expo.*, Mar. 2002, vol. 1, pp. 476–482.
[43] R. Z. Scapini, L. V. Bellinaso, and L. Michels, "Stability analysis of half-bridge rectifier employing LTP approach," in *Proc. 38th Annu. Conf. IEEE Ind. Electron Soc.*, Montreal, QC, Canada, Oct. 2012, pp. 780–785.

Rafael Z. Scapini (S'13) received the B.S. and M.S. degrees in electrical engineering, in 2010 and 2012, respectively, from the Federal University of Santa Maria, Santa Maria, Brazil, where he is currently working toward the Ph.D. degree.

Since 2014, he has been a Professor at the Federal Institute of Rio Grande do Sul, Ibirubá, Brazil. His current research interests include distributed generation, modeling and control of power converters, and applied digital control.

Lucas V. Bellinaso (S'12) received the B.S. and M.S. degrees in electrical engineering, in 2012 and 2014, respectively, from the Federal University of Santa Maria (UFSM), Santa Maria, Brazil, where he is currently working toward the Ph.D. degree.

Since 2015, he has been a Professor at UFSM. His current research interests include photovoltaic systems, modeling and control of power converters, and power/energy management of microgrids.

Leandro Michels (S'97–M'08) received the B.S. and Ph.D. degrees in electrical engineering from the Federal University of Santa Maria (UFSM), Santa Maria, Brazil, in 2002 and 2006, respectively.

Since 2009, he has been with the Power Electronics and Control Research Group, UFSM, where he is a Professor. He is the Technical Manager of Photovoltaic (PV) Inverter Testing Laboratory of GEPOC/UFSM. He has authored more than 70 technical papers. He holds three Brazilian patents. Since 2013, he has been a Fellow of Productivity in Technological Development and Innovative Extension (DT-1D) of CNPq/Brazil. In 2011, he was the General Chair of the 5th Power Electronics and Control Seminar, and in 2013, he was the Technical co-Chair of the 12th Brazilian Power Electronics Conference. His current research interests include PV systems, modeling and control of power electronic systems, and applied digital control.

Dr. Michels is a member of the administrative committee of the Brazilian Power Electronics Society.